Vibration–Based Fault Detection and Assessment in a Scale Aircraft Structure via Stochastic VFP-ARX Models

Fotis P. Kopsaftopoulos and Spilios D. Fassois

Stochastic Mechanical Systems & Automation (SMSA) Laboratory
Department of Mechanical & Aeronautical Engineering
University of Patras, GR 265 00 Patras, Greece
E-mail: {fkopsaf,fassois}@mech.upatras.gr
Internet: http://www.mech.upatras.gr/∼sms

ABSTRACT

The problem of vibration–based fault detection and assessment (localization and magnitude estimation) in a scale aircraft skeleton structure is addressed. The faults considered are of various magnitudes and occurrence locations, and are simulated by small masses added at various locations on the aircraft wing. The method postulated for tackling the problem is based upon novel Vector dependent Functionally Pooled AutoRegressive with eXogenous excitation (VFP-ARX) models, each one being capable of representing faults of all possible magnitudes and locations along a geometrical axis. The method generalizes the recently introduced Functional Model Based Method (FMBM), eliminating its limitations on fault occurrence location. It also allows for simultaneous fault detection, localization and magnitude estimation, for the accounting of uncertainties, and for operation even on a single pair of measurements. Its effectiveness and accuracy are illustrated via a series of laboratory experiments.

INTRODUCTION

The interest in the ability to monitor a structure and detect damage at an early stage is pervasive throughout the mechanical, aerospace and civil engineering communities. In fact, the combined problems of early detection, identification (localization) and magnitude estimation of faults are of paramount importance, as prompt detection may lead to better dynamic performance, increased safety and proper maintenance [1].

Vibration-based time series type methods for fault detection and assessment are among the most accurate and effective [1–4]. They offer a number of potential advantages, such as no requirement for visual inspection, "automation" capability, "global" coverage (in the sense of covering large areas of the structure), and the ability to work at a "system level". Nevertheless, and despite the fact that they generally tend to treat fault detection effectively, problems are frequently encountered when it comes to fault identification (localization) and magnitude estimation.

3rd European Workshop on
Structural Health Monitoring (SHM 2006)
Granada, Spain, July 2006

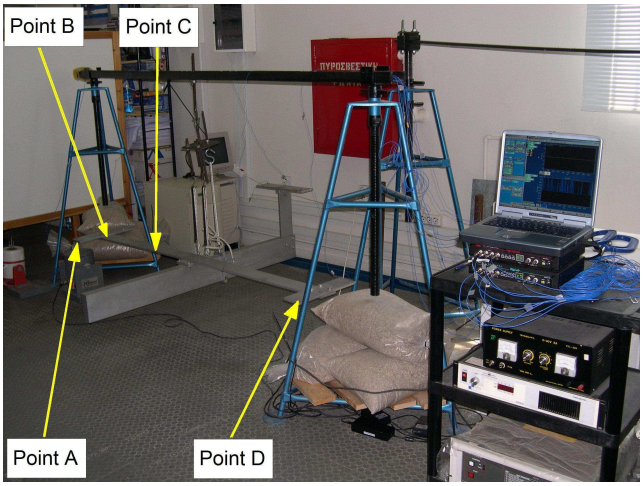

Figure 1. The aircraft skeleton structure and the experimental set-up: The force excitation (Point A) the vibration measurement positions (Points C and D), and the first fault location (Point B).

This paper addresses the combined problem of fault detection, identification and magnitude estimation in a prototype scale aircraft skeleton structure, with the emphasis being placed on the last two subproblems. This problem was recently tackled by the second author and his co-worker [5] via a Functional Model Based Method (FMBM). The objective of the present paper is a fresh look and re-tackling via an important generalization of the FMBM, which is now based upon novel *Vector dependent Functionally Pooled AutoRegressive with eXogenous excitation (VFP-ARX) models* [6]. These allow for the extension of the notion of *fault mode* to include faults not only of all possible magnitudes, but also, for the first time, of all possible *locations* along a geometrical axis. This results in straightforward fault localization and magnitude estimation, eliminating previous limitations on fault occurrence location. In addition, the method tackles the fault detection, identification and magnitude estimation subproblems within a unified framework, accounts for experimental and measurement uncertainties, and may operate even on a single pair of measurements.

THE EXPERIMENTAL SET-UP

The Structure. The scale aircraft structure considered was designed by ONERA in conjunction with the GARTEUR SM-AG19 Group, and manufactured at the University of Patras. It represents a typical aircraft design, and consists of six solid beams with rectangular cross sections representing the fuselage ($1500 \times 150 \times 50$ mm), the wing ($2000 \times 100 \times 10$ mm), the horizontal ($300 \times 100 \times 10$ mm) and vertical stabilizers ($400 \times 100 \times 10$ mm), and the right and left wing tips ($400 \times 100 \times 10$ mm). All parts are constructed from standard aluminium, and are jointed together via steel plates and screws. The total mass of the structure is approximately 50 kg.

The Faults. The faults considered are represented by small masses, which simu-

late local elasticity reductions, attached to nine successive locations (at distances of 10 cm) starting from Point B and moving left-wise along the right wing of the aircraft (Figure 1). The complete series covers the range of $[0, 80]$ cm along the wing. Each added mass weights approximately 8.132 gr, while up to 10 masses are used (representing different fault magnitudes), covering the range of $[0, 81.32]$ gr. Each fault is designated as $F^X_{k^1,k^2}$, with X indicating the fault mode (faults of all possible magnitudes and locations along an axis; presently the "right wing" fault mode is considered), k^1 the specific fault magnitude (gr of added mass) and k^2 the exact fault location (distance in cm from Point B). The healthy structure is designated as F_0.

The Experiments. Fault detection, identification and magnitude estimation are based upon vibration testing of the structure, which is suspended through a set of bungee cords under free-free boundary conditions.

The excitation is broadband random stationary Gaussian force applied vertically at the right wing tip (Point A, Figure 1) via an electromechanical shaker equipped with a stinger. The actual force exerted on the structure is measured via an impedance head, while the resulting vertical acceleration responses are measured at Points C and D (Figure 1) via lightweight (0.7 gr) accelerometers. The force and acceleration signals are driven through a conditioning charge amplifier into the data acquisition system based on two SigLab measurement modules.

A number of experiments are carried out, initially with the healthy structure and subsequently with the faulty, for each fault location and for the range of fault magnitudes. The acquired signals are digitized at 256 Hz (effective bandwidth 4-80 Hz), scaled (brought to common range), and mean-corrected. Each resulting signal is $N = 1000$ samples long.

THE VFP-ARX MODEL BASED METHOD

The *Vector dependent Functionally Pooled ARX (VFP-ARX)* model based method for combined fault detection, identification and magnitude estimation consists of two phases: (a) The *baseline phase*, which includes modelling of the fault modes considered (for the continuum of fault magnitudes and locations) via the novel class of stochastic VFP-ARX models. (b) The *inspection phase*, which is performed periodically during the structure's service cycle, and includes the functions of fault detection, identification and magnitude estimation.

Baseline Phase. A single experiment is performed, based upon which an interval estimate of a discrete-time dynamical model (or an array of models in the case of several vibration response measurement locations) representing the healthy structure's dynamics is obtained via standard identification procedures [7]. In the present study an array of two single-excitation single-response AutoRegressive with eXogenous excitation (ARX) models are used (each one for each vibration measurement location – Points C and D, Figure 1). This step is not strictly required, but it is customarily performed as it facilitates (providing approximate model orders) the subsequent step of fault mode modelling.

The modelling of the structure for a specific fault mode via VFP-ARX models involves consideration of all admissible fault magnitudes occurring at predetermined locations on a specific part of the structure (right/left wing, horizontal stabilizer, and so on). For this reason a total of $M_1 \times M_2$ experiments is performed (physically or via simulation). Each experiment is characterized by a specific fault magnitude k^1 and a specific fault location k^2, with the complete series covering the required range of each variable, say $[k^1_{min},\ k^1_{max}]$ and $[k^2_{min},\ k^2_{max}]$, via the discretizations $k^1 = k^1_1, k^1_2, \ldots, k^1_{M_1}$ and $k^2 = k^2_1, k^2_2, \ldots, k^2_{M_2}$ (it is tacitly assumed, without loss of generality, that the healthy structure corresponds to $k^1 = 0$).

For the identification of a model corresponding to a specific fault mode the vector parameter $\boldsymbol{k}$ is defined as:

$$\boldsymbol{k} \triangleq [k^1_i\ k^2_j]^T \Longleftrightarrow k_{i,j}, \quad i = 1, \ldots, M_1, \quad j = 1, \ldots, M_2 \tag{1}$$

with $k_{i,j}$ designating the state of the structure corresponding to the i-th fault magnitude and the j-th fault location.

The above procedure yields a series of excitation – response signal pairs (each of length N):

$$x_{\boldsymbol{k}}[t], y_{\boldsymbol{k}}[t] \ \text{ with } t = 1, \ldots, N,\ k^1 \in \{k^1_1, \ldots, k^1_{M_1}\},\ k^2 \in \{k^2_1, \ldots, k^2_{M_2}\} \tag{2}$$

with t representing normalized discrete time.

A proper mathematical description of the structure for the considered fault mode may be then obtained in the form of a VFP-ARX model. In the case of several vibration measurement locations, an array of such models may be obtained, with each scalar model corresponding to each measurement location and being designated as $F^{XY}_{\boldsymbol{k}}$ (X indicating the fault mode and Y the vibration measurement location).

The VFP-ARX model structure [6] postulated is of the form[1]:

$$y_{\boldsymbol{k}}[t] + \sum_{i=1}^{na} a_i(\boldsymbol{k}) \cdot y_{\boldsymbol{k}}[t-i] = \sum_{i=0}^{nb} b_i(\boldsymbol{k}) \cdot x_{\boldsymbol{k}}[t-i] + e_{\boldsymbol{k}}[t] \tag{3}$$

$$e_{\boldsymbol{k}}[t] \sim \ \text{iid}\, \mathcal{N}\big(0, \sigma^2_e(\boldsymbol{k})\big) \quad \boldsymbol{k} \in \mathbb{R}^2 \tag{4}$$

$$a_i(\boldsymbol{k}) \triangleq \sum_{j=1}^{p} a_{i,j} \cdot G_j(\boldsymbol{k}), \quad b_i(\boldsymbol{k}) \triangleq \sum_{j=1}^{p} b_{i,j} \cdot G_j(\boldsymbol{k}) \tag{5}$$

with na, nb designating the AutoRegressive (AR) and eXogenous (X) orders, respectively, $x_{\boldsymbol{k}}[t]$, $y_{\boldsymbol{k}}[t]$ the excitation and response signals, respectively, and $e_{\boldsymbol{k}}[t]$ the model's one-step-ahead prediction error (residual) sequence, that is a white (serially uncorrelated), Gaussian, zero-mean sequence with variance $\sigma^2_e(\boldsymbol{k})$ (hence iid, that is identically independently distributed, sequence), which is potentially cross-correlated with its counterparts corresponding to different experiments.

As Eq. (5) indicates, the AR and X parameters $\alpha_i(\boldsymbol{k}),\ b_i(\boldsymbol{k})$ are explicit functions of the vector $\boldsymbol{k}$ by belonging to a p-dimensional functional subspace spanned by the (mutually independent) functions $G_1(\boldsymbol{k}), G_2(\boldsymbol{k}), \ldots, G_p(\boldsymbol{k})$ (*functional basis*). The

[1]Lower case/capital bold face symbols designate vector/matrix quantities, respectively.

functional basis consists of polynomials of two variables (vector polynomials) obtained as tensor products from univariate polynomials (of the Chebyshev or other families). The constants $a_{i,j}$, $b_{i,j}$ designate the AR and X, respectively, coefficients of projection.

The VFP-ARX model of Eqs. (3)-(5) is parameterized in terms of the parameter vector (to be estimated from the measured signals) $\bar{\boldsymbol{\theta}} \triangleq [\ \alpha_{i,j} \vdots\ b_{i,j} \vdots \sigma_e^2(\boldsymbol{k})\ ]^T\ \forall\ \boldsymbol{k} \in \mathbb{R}^2$ and is re-written as:

$$y_{\boldsymbol{k}}[t] = \left[\boldsymbol{\varphi}_{\boldsymbol{k}}^T[t] \otimes \boldsymbol{g}^T(\boldsymbol{k})\right] \cdot \boldsymbol{\theta} + e_{\boldsymbol{k}}[t] = \boldsymbol{\phi}_{\boldsymbol{k}}^T[t] \cdot \boldsymbol{\theta} + e_{\boldsymbol{k}}[t] \tag{6}$$

with:

$$\begin{aligned}
\boldsymbol{\varphi}_{\boldsymbol{k}}[t] &\triangleq \left[-y_{\boldsymbol{k}}[t-1]\ \ldots\ -y_{\boldsymbol{k}}[t-na] \vdots x_{\boldsymbol{k}}[t]\ \ldots\ x_{\boldsymbol{k}}[t-nb]\right]^T_{[(na+nb+1)\times 1]} \\
\boldsymbol{g}(\boldsymbol{k}) &\triangleq \left[G_1(\boldsymbol{k})\ \ldots\ G_p(\boldsymbol{k})\right]^T_{[p\times 1]} \\
\boldsymbol{\theta} &\triangleq \left[a_{1,1}\ \ldots\ a_{na,p} \vdots\ \ b_{0,1}\ \ldots\ b_{nb,p}\right]^T_{[(na+nb+1)p\times 1]}
\end{aligned}$$

and ^{T} designating transposition and $\otimes$ Kronecker product.

Pooling together the expressions of the VFP-ARX model [Eq. (6)] corresponding to all parameter vectors $\boldsymbol{k}$ $(k_{1,1}, k_{1,2}, \ldots, k_{M_1,M_2})$, and following substitution of the data for $t = 1, \ldots, N$, the following expression is obtained [6]:

$$\boldsymbol{y} = \boldsymbol{\Phi} \cdot \boldsymbol{\theta} + \boldsymbol{e}. \tag{7}$$

The projection coefficient vector may be then estimated via a Weighted Least Squares (WLS) criterion, $J_{WLS} \triangleq \frac{1}{N}\boldsymbol{e}^T\boldsymbol{\Gamma}_{\boldsymbol{e}}^{-1}\boldsymbol{e}$, which leads to the Weighted Least Squares estimator [6]:

$$\hat{\boldsymbol{\theta}}_{WLS} = \left[\boldsymbol{\Phi}^T\boldsymbol{\Gamma}_{\boldsymbol{e}}^{-1}\boldsymbol{\Phi}\right]^{-1}\left[\boldsymbol{\Phi}^T\boldsymbol{\Gamma}_{\boldsymbol{e}}^{-1}\boldsymbol{y}\right]. \tag{8}$$

In these expressions $\boldsymbol{\Gamma}_{\boldsymbol{e}}$ designates the residual covariance matrix which is practically unavailable. Nevertheless, it may be consistently estimated by applying (in an initial step) Ordinary Least Squares (details in [6]). Once $\hat{\boldsymbol{\theta}}_{WLS}$ has been obtained, the residual variance final estimate is obtained as $\hat{\sigma}_e^2(\boldsymbol{k}, \hat{\boldsymbol{\theta}}_{WLS}) = \frac{1}{N}\sum_{t=1}^{N} e_{\boldsymbol{k}}^2[t, \hat{\boldsymbol{\theta}}_{WLS}]$.

Inspection Phase. Let $x[t], y[t]$ $(t = 1, \ldots, N)$ represent the excitation and response signals, respectively, obtained from the structure in a *current* (unknown) state.

Fault detection and assessment may be based upon the re-parameterized, in terms of $\boldsymbol{k}, \sigma_e^2(\boldsymbol{k})$ (keeping the projection coefficients at their previously estimated values), VFP-ARX model of any fault mode:

$$\mathcal{M}(\boldsymbol{k}, \sigma_e^2(\boldsymbol{k})): \quad y[t] + \sum_{i=1}^{na} a_i(\boldsymbol{k}) \cdot y[t-i] = \sum_{i=0}^{nb} b_i(\boldsymbol{k}) \cdot x[t-i] + e[t] \tag{9}$$

The estimation of the currently unknown parameters $\boldsymbol{k}, \sigma_e^2(\boldsymbol{k})$ based upon the current excitation – response signals may be achieved via the Nonlinear Least Squares (NLS) and the variance estimators:

$$\hat{\boldsymbol{k}} \triangleq \arg\min_{\boldsymbol{k}} \sum_{t=1}^{N} e^2[t]\ , \qquad \sigma_e^2(\hat{\boldsymbol{k}}) = \frac{1}{N}\sum_{t=1}^{N} e^2[t, \hat{\boldsymbol{k}}] \tag{10}$$

the first one realized via a hybrid optimization scheme based on Genetic Algorithms and constrained nonlinear optimization (sequential quadratic programming).

The first estimator may be shown (similarly to [5]) to be asymptotically Gaussian distributed, with mean equal to the true $\boldsymbol{k}$ value and covariance matrix $\boldsymbol{\Sigma_k}$ ($\hat{\boldsymbol{k}} \sim \mathcal{N}(\boldsymbol{k}, \boldsymbol{\Sigma_k})$) coinciding with the Cramer–Rao lower bound. Since the healthy structure corresponds to $k^1 = 0$ (zero fault magnitude), fault detection may be based upon the hypothesis testing problem:

$$\begin{aligned} H_0 &: k^1 = 0 \quad \text{(healthy structure)} \\ H_1 &: k^1 \neq 0 \quad \text{(faulty structure)} \end{aligned}$$

Under the null (H_0) hypothesis, the following statistic follows $t-$distribution with $N-2$ degrees of freedom [3]:

$$t = \frac{\hat{k}^1}{\hat{\sigma}_{k^1}} \sim t(N-2) \tag{11}$$

with $\hat{\sigma}_{k^1}$ being the positive square root of the first diagonal element of $\widehat{\boldsymbol{\Sigma}}_{\boldsymbol{k}}$ (estimated standard deviation of k^1). This leads to the following test at the α risk level (probability of false alarm, or type I error, that is accepting H_1 although H_0 is true, being equal to α):

$$\begin{aligned} t_{\frac{\alpha}{2}}(N-2) \leq t \leq t_{1-\frac{\alpha}{2}}(N-2) &\implies H_0 \text{ is accepted} \quad \text{(healthy structure)} \\ \text{Else} &\implies H_1 \text{ is accepted} \quad \text{(faulty structure)} \end{aligned}$$

with t_α designating the t distribution's α critical point.

Once fault occurrence has been detected, current fault mode determination is based upon the successive estimation and validation of the re-parameterized VFP-ARX models. The procedure stops as soon as a particular model is successfully validated, with the corresponding fault mode identified as the current (as in [5]).

Fault identification (localization) and magnitude estimation are then based upon the interval estimates of k^2 and k^1, respectively, which are constructed based on the $\hat{\boldsymbol{k}}, \widehat{\boldsymbol{\Sigma}}_{\boldsymbol{k}}$ estimates obtained from the corresponding re-parameterized VFP-ARX model (of the form of Eq. (9)) of the *current* fault mode. Thus, using Eq. (11), the interval estimates of k^1 (fault magnitude) and k^2 (fault location) at the α risk level are:

$$k^i \quad \text{interval estimate:} \qquad \left[\hat{k}^i + t_{\frac{\alpha}{2}}(N-2) \cdot \hat{\sigma}_{k^i},\ \hat{k}^i + t_{1-\frac{\alpha}{2}}(N-2) \cdot \hat{\sigma}_{k^i}\right] \tag{12}$$

with $i = 1$ for fault magnitude and $i = 2$ for fault location, while $\hat{\sigma}_{k^i}$ is the positive square root of the i-th diagonal element of $\widehat{\boldsymbol{\Sigma}}_{\boldsymbol{k}}$.

Bivariate confidence bounds for $\boldsymbol{k} = [k^1\, k^2]^T$ may be also obtained by observing that the quantity:

$$(\widehat{\boldsymbol{k}} - \boldsymbol{k})^T {\boldsymbol{\Sigma_k}}^{-1} (\widehat{\boldsymbol{k}} - \boldsymbol{k}) \sim \chi^2(2) \tag{13}$$

(follows chi-square distribution with two degrees of freedom). Thus the probability that:

$$(\widehat{\boldsymbol{k}} - \boldsymbol{k})^T {\boldsymbol{\Sigma_k}}^{-1} (\widehat{\boldsymbol{k}} - \boldsymbol{k}) \leq \chi^2_{1-\alpha} \tag{14}$$

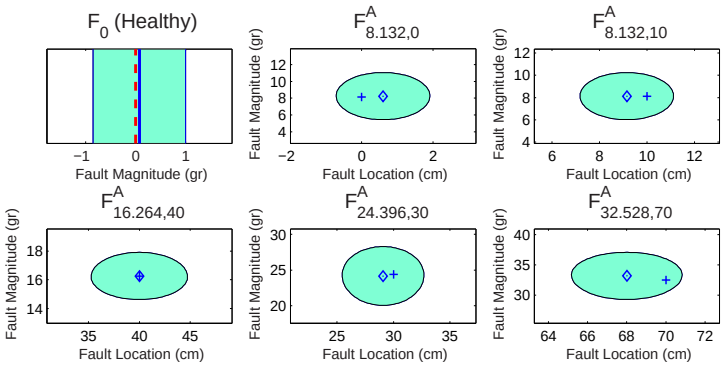

Figure 2. Fault detection, localization and magnitude estimation results for six test cases (the correct fault indicated above the plot; for the first test case the confidence bound of only the fault magnitude is depicted; for the other test cases the bivariate confidence bounds are depicted at the $\alpha = 0.05$ risk level [+: true values, $\diamond$: point estimates]).

is equal to $1 - \alpha$ ($\chi^2_{1-\alpha}$ designating the χ^2 distribution's $1 - \alpha$ critical point). The above expression represents the area inside an ellipsoid on the (k^1, k^2) plane, which defines the (k^1, k^2) bivariate confidence bound at the α risk level (notice that in practice $\boldsymbol{\Sigma_k}$ is replaced by its estimate, which is currently assumed to be of negligible variability).

EXPERIMENTAL RESULTS

Baseline Phase. Fault mode modelling, for the single fault mode (designated as $F^A_{k^1,k^2}$ or $F^A_{\boldsymbol{k}}$) defined as the union of faults (attached masses) of all possible magnitudes at the right wing of the aircraft, is based upon signals obtained from a total of $M_1 \times M_2 = 99$ experiments. 9 of these correspond to the healthy structure ($k^1 = 0$ gr) and 90 to the faulty structure (1–10 masses being placed at each one of the 9 locations on the right wing). The mass and location increments used are $\delta k^1 = 8.132$ gr and $\delta k^2 = 10$ cm, and the ranges of $[0, 81.32]$ gr and $[0, 80]$ cm (starting from Point B and moving left-wise; Figure 1) are covered.

Two VFP-ARX fault mode models, based on the vibration measurement at Points C and D and designated as $F^{AC}_{\boldsymbol{k}}, F^{AD}_{\boldsymbol{k}}$, respectively, are constructed. The VFP-ARX modelling procedure based upon the N=1000 sample-long excitation–response signals leads to a VFP-ARX$(52, 52)$ model with functional basis consisting of $p = 12$ Chebyshev Type II vector polynomials (selected via a Genetic Algorithm) for point C, and a VFP-ARX$(51, 51)$ model with functional basis consisting of $p = 16$ vector polynomials for point D.

Inspection Phase. Six test cases, one corresponding to the healthy structure (F_0) and five to faults characterized by added masses attached to various locations on the right wing (not necessarily coinciding with those used in the baseline phase) are considered. The corresponding fault detection, identification and magnitude estimation results are pictorially presented in Figure 2. The first three test cases are based on

the $F^{AC}_{\boldsymbol{k}}$ fault mode model, whereas the latter three are based on the $F^{AD}_{\boldsymbol{k}}$ fault mode model.

In the first case (healthy structure, F_0) the interval estimate of only the fault magnitude (gr) is depicted. Evidently, no fault is detected as the interval estimate at the $\alpha = 0.05$ risk level (shaded strip) includes the $k^1 = 0$ value (this is equivalent to described test; notice that the dashed vertical line designates the true fault magnitude while the middle line the point estimate and the left and right vertical lines the lower and upper confidence bounds, respectively). In the rest of the cases the bivariate (k^1, k^2) confidence bounds (at the $\alpha = 0.05$ risk level) are depicted. A fault is, in each of these cases rightly detected as the fault magnitude's interval estimate does not include the $k^1 = 0$ value (vertical axis). It should be further observed that very accurate estimates of the fault magnitude and location, characterized by narrow confidence bounds, are obtained.

Acknowledgement

The authors acknowledge the funding of this work by the European Social Fund (ESF), Operational Program for Education and Vocational Training II (EPEAEK II), and particularly the program PYTHAGORAS II of the Greek Ministry of Education.

REFERENCES

1. Doebling, S.W., C.R. Farrar, M.B. Prime, and D.W. Shevitz. 1996. "Damage Identification and Health Monitoring of Structural and Mechanical Systems from Changes in Their Vibration Characteristics: A Literature Review", Report LA-13070-MS, Los Alamos National Laboratory, USA.
2. Zou, Y., L. Tong, and G.P. Steven. 2000. "Vibration-Based Model-Dependent Damage (Delamination) Identification and Health Monitoring for Composite Structures – A Review", *J. of Sound and Vibration*, 230(2):357-378.
3. Fassois, S.D. and J.S. Sakellariou. 2006. "Time Series Methods for Fault Detection and Identification in Vibrating Structures", *The Royal Society - Philosophical Transactions: Mathematical, Physical and Engineering Sciences*, to appear.
4. Basseville, M., M. Abdelghani, and A. Benveniste. 2000. "Subspace-Based Fault Detection Algorithms for Vibration Monitoring", *Automatica*, 36(1):101-109.
5. Sakellariou, J.S. and S.D. Fassois. 2004. "Fault Detection and Identification in a Scale Aircraft Skeleton Structure via a Functional Model Based Method", in *Proc. Intern. Conf. Noise and Vibration Engineering*, Leuven, pp. 515–529.
6. Kopsaftopoulos, F.P. and S.D. Fassois. 2006. "Identification of Stochastic Systems Under Multiple Operating Conditions: The Vector Dependent FP-ARX Parametrization", submitted to the *Mediterranean Conference on Control and Automation*, Ancona. Extended version to be submitted for journal publication.
7. Ljung, L. 1999. *System Identification: Theory for the User.* Second edition, Prentice-Hall.